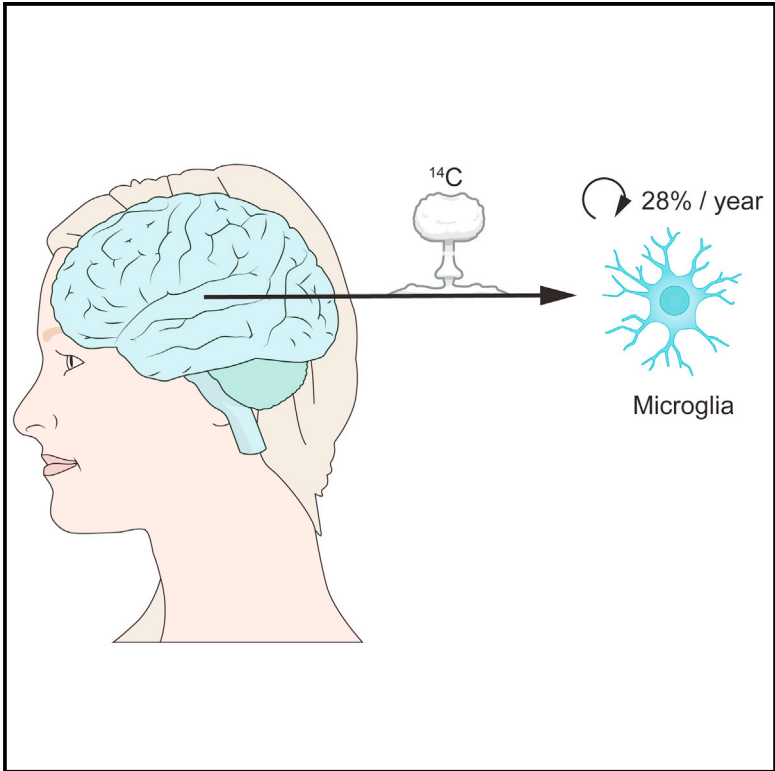


The Lifespan and Turnover of Microglia in the Human Brain

Graphical Abstract



Authors

Pedro Réu, Azadeh Khosravi, Samuel Bernard, ..., Göran Possnert, Henrik Druid, Jonas Frisen

Correspondence

jonas.frisen@ki.se

In Brief

Taking advantage of the decreasing level of atmospheric ^{14}C since the Cold War, Réu et al. show that human microglia, unlike most other hematopoietic lineages, slowly turn over at a yearly median rate of 28%. The absence of a large quiescent subpopulation indicates that most microglia will renew throughout life.

Highlights

- Human microglia renew at a median rate of 28% per year
- Microglial cells are on average 4.2 years old
- Most of the microglia population (>96%) is renewed throughout life



The Lifespan and Turnover of Microglia in the Human Brain

Pedro Réu,^{1,2} Azadeh Khosravi,¹ Samuel Bernard,³ Jeff E. Mold,¹ Mehran Salehpour,⁴ Kanar Alkass,^{1,5} Shira Perl,⁶ John Tisdale,⁶ Göran Possnert,⁴ Henrik Druid,⁵ and Jonas Frisen^{1,7,*}

¹Department of Cell and Molecular Biology, Karolinska Institute, SE-171 77 Stockholm, Sweden

²Center for Neuroscience and Cell Biology, University of Coimbra, 3004-517 Coimbra, Portugal

³Institut Camille Jordan, CNRS UMR 5208, University of Lyon, 69622 Villeurbanne, France

⁴Department of Physics and Astronomy, Ion Physics, Uppsala University, 751 20 Uppsala, Sweden

⁵Department of Forensic Medicine, Karolinska Institutet, 171 77 Stockholm, Sweden

⁶NHLBI, NIH, Bethesda, MD 20892, USA

⁷Lead Contact

*Correspondence: jonas.frisen@ki.se

<http://dx.doi.org/10.1016/j.celrep.2017.07.004>

SUMMARY

The hematopoietic system seeds the CNS with microglial progenitor cells during the fetal period, but the subsequent cell generation dynamics and maintenance of this population have been poorly understood. We report that microglia, unlike most other hematopoietic lineages, renew slowly at a median rate of 28% per year, and some microglia last for more than two decades. Furthermore, we find no evidence for the existence of a substantial population of quiescent long-lived cells, meaning that the microglia population in the human brain is sustained by continuous slow turnover throughout adult life.

INTRODUCTION

Microglia are the resident macrophages of the CNS, which dynamically survey their surrounding for signs of infection or cell distress (Casano and Peri, 2015). In mice, microglial progenitor cells derive from an early myeloid branch of the hematopoietic lineage in the embryonic yolk sac and enter the CNS before the blood-brain barrier is formed (Ginhoux et al., 2010; Schulz et al., 2012). There is no further contribution from the peripheral hematopoietic system under physiological conditions, and this is a self-sustaining population within the CNS (Ajami et al., 2007; Askew et al., 2017; Bruttger et al., 2015; Hoeffel et al., 2015; Mildner et al., 2007). The self-contained nature of this population makes it vulnerable to local disturbances. Additionally, it is key for brain homeostasis that microglial cell numbers are stably maintained, because having reduced numbers results in behavioral and learning deficits (Parkhurst et al., 2013).

Based on [³H]thymidine incorporation, heavy water (²H₂O) labeling, and 5-ethynyl-2'-deoxyuridine (EdU) and 5-bromo-2'-deoxyuridine (BrdU) incorporation, 0.075%–1.04% of microglia in adult mice of different strains and 2.35% of microglia in the young adult macaque were estimated to enter the cell cycle each day (Askew et al., 2017; Lawson et al., 1992; Shankaran et al., 2007; Tay et al., 2017; Tonchev et al., 2003). It is difficult

to infer cell turnover dynamics in humans from data in experimental animals, which may have very different requirements or lifespans. Assessing the turnover of human immune cells is notably important because it is particularly hard to deduce renewal rates from laboratory animals, which live in pathogen-free barrier facilities (Beura et al., 2016). A recent study demonstrated that 2% of microglia in the adult human brain are in cell cycle at any given time based on Ki-67 labeling, but the authors noted the limitations of this approach and acknowledge the need for more precise measurements (Askew et al., 2017). It is difficult to estimate cell turnover dynamics based on cell cycle markers, because it rests on assumptions of cell cycle length. Moreover, it is not possible to know whether the cell will proceed through the cell cycle to mitosis or whether the potential progeny will survive.

RESULTS

We analyzed the frontal and occipital cortices from two subjects (17 and 41 years old) who had received IdU (5-Iodo-2'-deoxyuridine) as a radiosensitizer for cancer treatment (Table S1). On average, 0.8% of Iba1⁺ parenchymal microglia in the cortex were IdU⁺ after 4 days (donor 1) or 10 days (donor 2) of IdU administration (Figures 1A and 1B; Table S1). Accounting for the labeling period, it averages at 0.14% labeling per day (Figure 1C). These observations do, however, come with the following caveats: (1) the sample size is small and additional samples are not available; and (2) the subjects studied are not healthy individuals, and thus may exhibit aberrant turnover of different populations of cells. Still, our observations provide us with a general estimate of what to expect in our downstream analysis based on retrospective ¹⁴C measurements.

Following CD11b magnetic bead selection, we isolated by fluorescence-activated cell sorting (FACS) CD45⁺/CD11b⁺ microglia from the adult human postmortem cerebral cortex in order to perform retrospective ¹⁴C dating (Figures 2A–2C) (Olah et al., 2012). We used CD20, a B cell marker, to evaluate the presence of blood-borne cells in dissociated cortical preparations. The percentage of B cells in brain samples prior to MACS purification (Figure 2D) is very low relative to the circulation

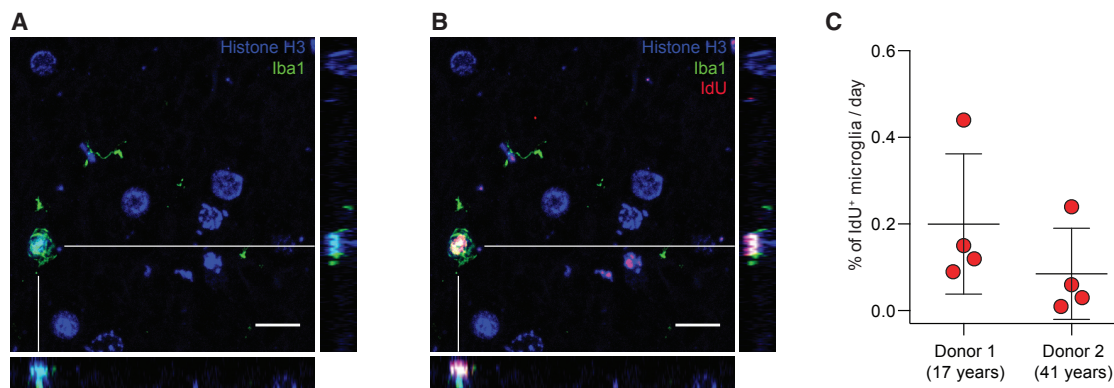


Figure 1. IdU Incorporation

(A) Confocal image with orthogonal projections, from human cortex, revealing microglia positive for Iba1.

(B) Co-staining of Iba1 and the thymidine analog IdU.

(C) Percentage of microglia incorporating IdU per day (mean \pm SD). Each data point represents a glass slide. Nuclei are labeled with antibodies to histone H3. Scale bars, 10 μ m.

(Figure 2E), indicating that contamination by blood-borne cells is likely to be a negligible factor. The average postmortem interval of our donors is 43 hr, and it is likely that most blood has coagulated inside the vessels. Nonetheless, we decided to experimentally address the possible contamination with peripheral monocytes, which also express CD45 and CD11b. To do so, we isolated CD11b⁺ cells from peripheral blood with magnetic beads, following the same positive selection protocol we used to isolate microglia from dissociated cortical specimens, and labeled them with carboxyfluorescein succinimidyl ester (CFSE). We then prepared a mixed sample containing both CD11b⁺/CFSE⁺ blood cells and CD11b⁺ microglia isolated in parallel (Figure 2F). This allowed us to simultaneously label and visualize both populations in a single sample, ruling out variability in labeling protocols. Microglia were found to exhibit lower expression of CD45 and did not overlap with blood-borne cells, further suggesting that cells from the blood are not likely to be a significant source of contamination, because cells with higher CD45 expression were excluded in all experiments (Figure 2G). We confirmed the identity of the isolated microglial cells by qPCR using Iba1, CD11b, and CD45 (Tambuyzer et al., 2009), and found only minimal contamination of neurons (NeuN), astrocytes (GFAP), or oligodendrocytes (MBP) (Figure 2H). As expected, the sorted cells are positive for the microglial marker Iba-1 (Figure 2I).

By relating the ¹⁴C level in the DNA of cells to the atmospheric ¹⁴C curve, one can determine the average date of birth of the cell population (Spalding et al., 2005) (Figure 3A). Using this strategy, we performed retrospective birth dating of microglia isolated from adults born across six decades (Figure 3B; Table S2). Based on the year of collection and date of birth of the sample, it is possible to calculate the average cell age of the sample (Figure 3C). Using a homogeneous turnover model in which each cell is replaced at a fixed rate, it is possible to obtain robust snapshots of cell dynamics for each individual donor (Bernard et al., 2010). In simple terms, this is accomplished by calculating how often cells need to divide within an individual of a given age in or-

der for the cells to have the measured ¹⁴C level. If cells are as old as the individual, their renewal rate is zero and the measured ¹⁴C level corresponds to the level at birth. In mice, under homeostatic conditions, microglia have been shown to have a stable network and to self-renew stochastically (Tay et al., 2017). Similarly, in the homogeneous turnover model, all cells are equally likely to be replaced (Supplemental Information). Our results indicate that the majority of microglia in the healthy human cortex are replaced by newly produced cells at a median rate of 28% per year (or 0.08% per day), and that they have an average age of 4.2 years (Figure 3C; Table S2). This is a lower rate than estimated by IdU incorporation (0.14% per day; Figure 1C). The difference may indicate that the microglial population is somewhat heterogeneous because a pulse of IdU preferentially labels a more rapidly dividing subpopulation.

Cells that became postmitotic soon after birth have a unique ¹⁴C signature, corresponding to the atmospheric level at that moment in time. This allowed us to directly investigate the possible existence of a non-dividing subpopulation, using a heterogeneous turnover model (Figure 3D). The model that best fits our data are one where the majority of the population (>96%) is renewed and we have no evidence to support the existence of a significant subpopulation of quiescent very long-lived cells (Figure 3D). We have employed a conservative mathematical model, with few assumptions, which does not preclude that an extended dataset or other variables could explain the heterogeneity observed.

Based on the average cell age and cell division rate observed, we generated cell age distributions stochastically, showing that within an individual there is a wide range of microglia ages (Figure 3E). Simply because not all cells are dividing at the same time, some are quite young due to recent cell division and others can be more than 20 years old (Figure 3E).

The lower rate of microglia renewal compared with most other immune cells is probably a manifestation of the immune-privileged status of the CNS (Figure 3F) (Busch et al., 2007; Macallan et al., 2005). On the other hand, in comparison with other cells of

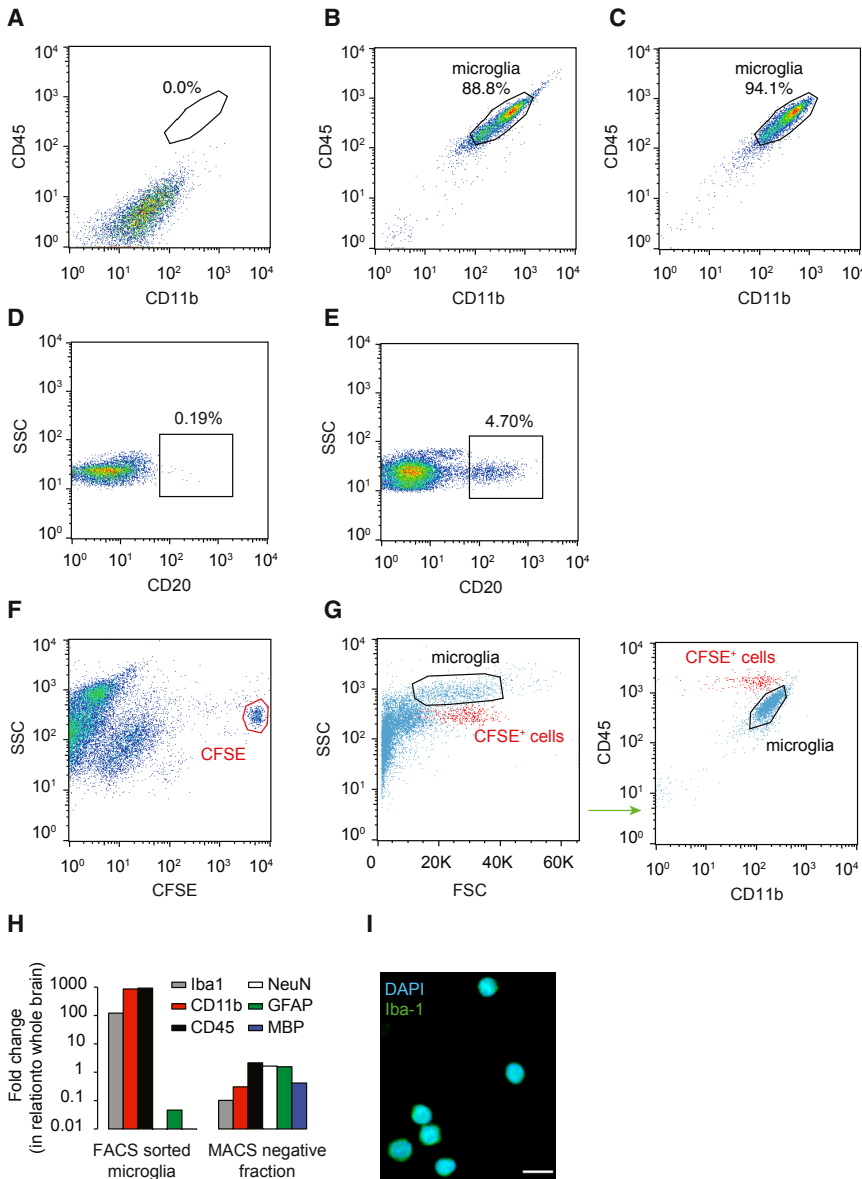


Figure 2. Microglia Isolation

(A) Unstained brain single-cell suspension following CD11b isolation with magnetic beads. (B) Sorting gate for FACS sorting of stained microglial cells. (C) Representative post-sort purity of microglia sample. (D) FACS plot representing the percentage of positive cells for the B cell marker CD20 in a brain sample prior to MACS purification. (E) FACS plot representing the percentage of positive cells for CD20 in a sample of peripheral blood. (F) Blood cells were positively selected with CD11b microbeads, labeled with CFSE (red gate), and then spiked into a brain preparation previously selected with CD11b microbeads. (G) Gating strategy for the sorting of microglia (spiked blood cells in red). (H) qRT-PCR reveals that, when compared with the magnetic bead negative fraction, the FACS sorted microglia sample is several hundred-fold enriched for mRNA of the microglia markers Iba1, CD11b, and CD45 and depleted of mRNA for markers of neurons (NeuN), astrocytes (GFAP), and oligodendrocytes (MBP). (I) FACS sorted cells are positive for the microglial marker Iba-1 (A488). Scale bar, 10 μ m.

renewal in humans (Eriksson et al., 1998; Ernst et al., 2014; Yeung et al., 2014).

Analysis of the integration of atmospheric 14 C, derived from nuclear bomb tests, in genomic DNA is cumulative and gives a more comprehensive view of cell age and cell division history (Spalding et al., 2005), and it is possible to analyze tissue from subjects without previous serious illness. There is little exchange of carbon atoms in genomic DNA in non-dividing cells, and the effect of DNA repair and methylation is well below the detection limit of this retrospective birth dating strategy (Bergmann et al., 2012; Ernst et al., 2014; Spalding et al., 2005),

the CNS, microglia show a high exchange rate (Figure 3F) (Spalding et al., 2005, 2013; Yeung et al., 2014). Thus, a constant basal renewal is likely necessary for the maintenance of a cohort of young and healthy microglial cells.

DISCUSSION

Administering nucleotide analogs for a short time period introduces a bias to label the cells with the highest proliferation rate within a potentially heterogeneous population. Also, labeled cells that continue to proliferate after the labeling period will give rise to additional positively labeled cells that lead to overestimations of cell proliferation (Neese et al., 2002). Nevertheless, samples of human brain labeled with nucleotide analogs are very valuable, not only due to their rarity but also as a confirmatory tool of in vivo

even after, for example, stroke, where there is a substantial increase in DNA damage and repair (Huttner et al., 2014).

Most immune cells do not live longer than a few days or weeks (Busch et al., 2007; Macallan et al., 2005), making microglia one of the slowest dividing immune cells described to date. An extreme exception is plasma cells in the intestine, where the subset with the slowest renewal rate has a median age of 22 years (Landsverk et al., 2017). The turnover rate of microglia in humans is substantially lower than in mice. There is a much higher exchange of oligodendrocytes in mice compared with humans (Yeung et al., 2014), and it is possible that clearance of myelin and cell debris calls for a higher exchange rate of microglia in mice.

Based on Ki-67 staining, a recent study estimated that, at any given moment, 2% of microglia are proliferating in the

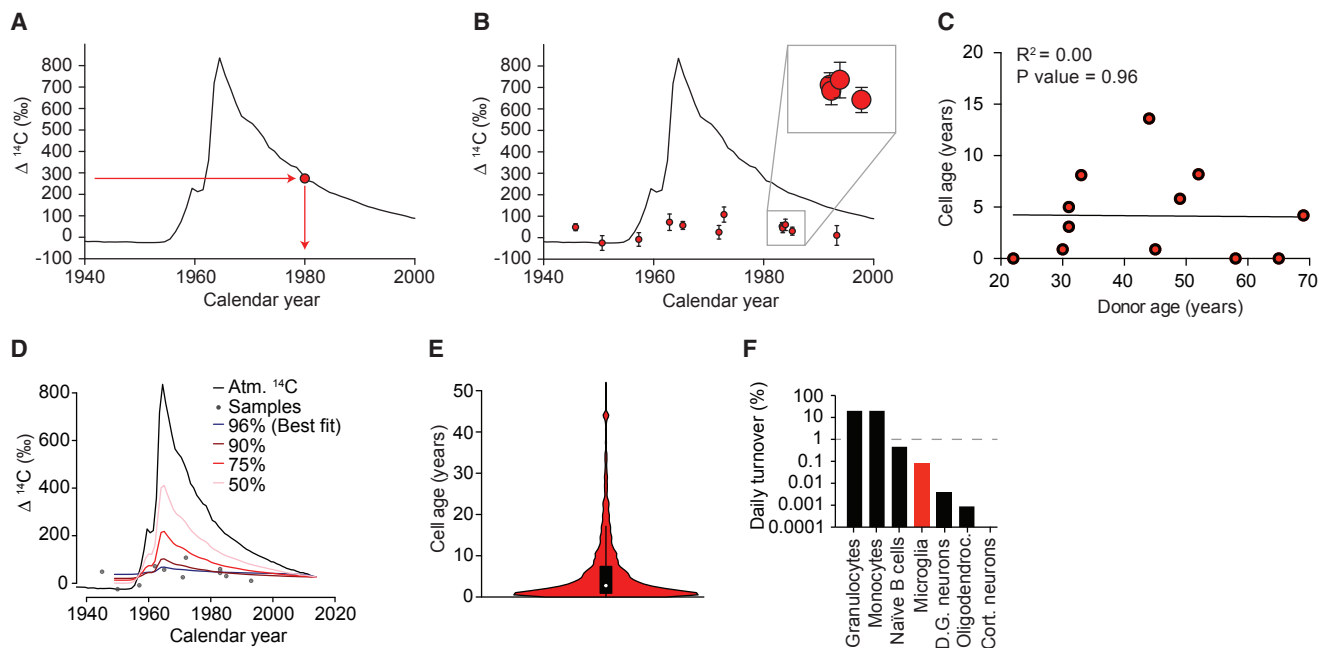


Figure 3. Microglial Population Dynamics

(A) Schematic illustration of the ^{14}C atmospheric curve over time (Levin et al., 2010). The concentration of ^{14}C in the genomic DNA of a cell population is dependent on the atmospheric ^{14}C concentration (y axis). Thus, the birth date of the cell population can be read off the x axis.

(B) ^{14}C content in the genomic DNA of human cortical microglia from donors born across six decades. Data points plotted along the x axis according to the date of birth of the donors. Close-up view of four nearly overlapping data points (gray square). The error bars represent the ^{14}C concentration measurement error.

(C) Representation of the average age of microglia in each individual and linear regression (black line).

(D) Different models for distribution of data on the atmospheric ^{14}C curve considering different frequencies of dividing cells. The model that best fits the data are one where most cells (>96%) renew.

(E) Considering the turnover rate, the average cell age, and the fact that all microglial cells do not divide simultaneously, we created a stochastic cell age distribution model. Our model shows that within an individual there is a distribution of cells of different ages, with some having recently renewed and others not having divided in more than 20 years (donors with infinite turnover not included).

(F) The approximate rate of microglia turnover is 0.08% a day, a low turnover rate in comparison with other immune cells (granulocytes, monocytes, and naive B cells) but a high turnover rate relative to other CNS cells (neurons in the dentate gyrus, oligodendrocytes, and cortical neurons).

human brain (Askew et al., 2017). Similarly to short-term labeling experiments using BrdU or IdU, Ki-67 staining detects dividing cells, but it provides limited information for cells that may exhibit slow renewal rates. Importantly, Ki-67 does not measure proliferation directly, and cells blocked in G_1 or destined to enter apoptosis can accumulate in the population as Ki-67⁺ events because of a G_1/S block (Busch et al., 2007). An additional explanation for the results of the different techniques resides in the fact that newborn microglia are more likely to die than the resident microglia (Askew et al., 2017). Hence, many of the cells detected by Ki-67 and, to a lesser extent, by IdU may be destined to die and not to replace existing ones.

In conclusion, ^{14}C analyses reveal that microglia as a whole turn over slowly, and that individual cells can potentially be decades old. Complementary, IdU and Ki-67 (Askew et al., 2017) measurements suggest heterogeneity within the population possibly induced by the presence of a subpopulation of fast dividing cells. Finally, our data predict a nearly complete renewal of the microglia population in the human cortex during the lifespan of an individual, similar to what has been seen in mice (Askew et al., 2017).

EXPERIMENTAL PROCEDURES

Tissue Collection

Neocortical tissue was obtained from donors admitted for autopsy at the Department of Forensic Medicine in Stockholm from 2014 to 2016, after informed consent from the relatives. The ethical permit for this study was granted by the Regional Ethics Committee of Stockholm (2010/313-31/3). Formalin-fixed and paraffin-embedded sections of cortical frontal lobe and occipital lobe from cancer patients, who had received IdU for therapeutic purposes, were obtained from the National Heart, Lung and Blood Institute, NIH. Buffy coats were obtained from anonymous regular blood donors at Blodcentralen, Karolinska University Hospital.

IdU Quantification

The sections were immersed in xylene to remove the paraffin, and the tissue was rehydrated in descending ethanol series. Triton X-100 (0.2%) was used to permeabilize the tissue, and antigen retrieval was performed in 0.05% citraconic acid solution (pH 7.4) for 20 min in a domestic steamer. The sections were left for 20 min at room temperature and then immersed in 2.0 N HCl for 40 min. The slides were blocked (10% donkey normal serum in PBS with 0.2% Triton X-100) at room temperature for 1 hr. Following incubation with the primary antibodies (1:60 mouse anti-BrdU, BD347580; 1:100 goat anti-Histone H3, Abcam 12079; 1:100 rabbit anti-Iba1, Wako 019-19741), the sections were incubated with the secondary antibodies (1:200 donkey anti-mouse Cy3, Jackson ImmunoResearch 715-165-150; 1:200 donkey anti-goat A647,

Jackson ImmunoResearch 705-605-147; 1:200 donkey anti-rabbit A488, Jackson ImmunoResearch 711-545-152) and inspected in an LSM 700 (Carl Zeiss) confocal microscope. The percentage of IdU⁺ microglia in each slide was found based on the total number of Iba⁺ cells and the number of Iba⁺/IdU⁺ cells. By dividing the percentage of labeled cells by the number of labeling days (4 for donor 1 and 10 for donor 2), we calculated the daily labeling. The raw data and the calculations are in [Table S1](#).

Tissue Dissociation

After careful removal of the meninges and all visible blood vessels, the tissue was cut into small pieces and thoroughly rinsed with PBS. The tissue was then homogenized in media A (1 × HBSS, 150 mM HEPES, 2 mM EDTA, 5% BSA) with 2 U/mL papain (Worthington) and 10 U/mL DNaseI (Roche) at 37°C for 1.5 hr. The homogenized tissue was mixed with 3 volumes of sucrose media I (PBS, 0.7 M sucrose, 2 mM EDTA) and centrifuged for 20 min at 1,000 × *g*. The pellet was then resuspended in sucrose media II (PBS, 0.9 M sucrose, 2 mM EDTA) and centrifuged for 25 min at 800 × *g*. Finally the pellet was resuspended in blocking solution (PBS, 0.1% FBS, 2 mM EDTA) and filtered through a 40 μm cell strainer.

Cell Isolation

The cell suspension was incubated for 5 min with human Fc-gamma receptor (FcR)-binding inhibitor (1:100; eBioscience) and for 30 min with CD11b antibody-conjugated microbeads (1:25, 130-093-634; Miltenyi Biotec). The magnetic isolation was performed according to the manufacturer. The samples were next incubated for 20 min with PE-CD11b (1:20, clone ICRF44; BioLegend) and Alexa 647 CD45 (1:20, clone HI30; BioLegend), and finally FACS sorted in an Influx flow cytometer (BD Biosciences). Blood cells were isolated from buffy coats by density gradient (Lymphoprep). Peripheral blood mononuclear cells (PBMCs) were positively selected with CD11b antibody-conjugated microbeads (1:25, 130-093-634; Miltenyi Biotec) according to the manufacturer.

DNA Isolation

In order to prevent carbon contaminations, we performed the DNA isolation in a clean room (ISO8). The extraction protocol was modified from [Miller et al. \(1988\)](#). The glassware was prebaked for 4 hr at 450°C. 1 mL of lysis buffer (100 mM Tris [pH 8.0], 200 mM NaCl, 1% SDS, and 5 mM EDTA) and 12 μL of Proteinase K (40 mg/ml) were added to the sorted cells and incubated at 65°C overnight. The samples were further incubated at 65°C for 1 hr after 6 μL of RNase cocktail (Ambion) was added. 600 μL of NaCl (5 M) was added to the sample; then it was vortexed for 30 s. The solution was spun down at 13,000 rpm for 6 min. The supernatant containing the DNA was transferred to a 12 mL glass vial. Ethanol 95% (6 mL) was added and the glass vial was manually agitated. The DNA precipitate was washed three times in DNA washing buffer (70% ethanol [v/v] and 0.5 M NaCl), dried at 65°C overnight, and resuspended in 0.5 mL DNase/RNase free water (GIBCO/Invitrogen). The DNA purity and concentration were verified by UV spectroscopy (NanoDrop).

Accelerator Mass Spectrometry

DNA samples suspended in 0.5 mL of water were lyophilized to dryness in a vacuum centrifuged at 2,000 rpm for 2 hr. To convert the samples into graphite, we added excess CuO to each dry sample, and the quartz tubes were evacuated and sealed with a high temperature torch. The tubes were placed in a furnace set at 900°C for 3 hr to combust all carbon to CO₂. The gas was then purified by freezing the residual water at -80°C, as well as cryogenically trapping the CO₂ at -196°C and discarding all the other gases. The CO₂ was chemically reduced to graphite in the presence of zinc powder and iron catalyst in individual miniaturized reactors at 550°C for 6 hr. Thorough laboratory protocols are exercised to minimize the introduction of stray carbon into the sample ([Salehpour et al., 2013a](#)). Graphite targets were pressed into individual cathodes and are measured at the Department of Physics and Astronomy, Ion Physics, Uppsala University ([Salehpour et al., 2013a, 2013b, 2015](#)) using the 5 MV Pelletron Tandem accelerator. Large CO₂ samples (>100 μg) may be split, and δ¹³C are measured by stable isotope ratio mass spectrometry, which established the δ¹³C correction to -24.1‰ ± 0.5‰ (1 SD), which was applied to the samples. Corrections for background carbon introduced during sample

preparation were made as described previously ([Salehpour et al., 2013a, 2013b, 2015](#)). The measurement error was determined for each sample and ranged between ±8‰ and 40‰ (2 SD) Δ¹⁴C for the large (>100 mg C) and small samples (10 μg C), respectively. All ¹⁴C data are reported as Fraction Modern F¹⁴C as defined in [Reimer et al. \(2004\)](#) or Δ¹⁴C as defined in [Stuiver and Polach \(1977\)](#). All accelerator mass spectrometry (AMS) analyses were performed blind to the identity of the sample.

qRT-PCR

qRT-PCR was performed using TaqMan gene expression assays (RBF0X3, 4331182; AIF-1, 4331182; ITGAM, 4331182; PTPRC, 4331182; GAPDH, 4331182; and MBP, 4331182).

SUPPLEMENTAL INFORMATION

Supplemental Information includes Supplemental Experimental Procedures and two tables and can be found with this article online at <http://dx.doi.org/10.1016/j.celrep.2017.07.004>.

AUTHOR CONTRIBUTIONS

P.R. and J.F. designed the study. P.R. performed most of the experiments. A.K. performed the IdU analyses. S.B. did all of the mathematical analyses. J.E.M. performed additional experiments. M.S. and G.P. did the AMS measurements. K.A. and H.D. collected and classified the samples for ¹⁴C. S.P. and J.T. collected and classified the IdU samples. P.R., J.E.M., and J.F. wrote the manuscript.

ACKNOWLEDGMENTS

We are grateful to Marcelo Toro and Sarantis Giatrellis for help with flow cytometry, the staff at the Swedish National Board of Forensic Medicine for procuring tissue, and Karl Håkansson and Peter Senneryd for AMS sample preparation. This study was supported by grants from the Swedish Research Council, the Swedish Cancer Society, the Karolinska Institute, Tobias Stiftelsen, the ERC, Knut och Alice Wallenbergs Stiftelse, and Torsten Söderbergs Stiftelse. P.R. was supported by the Portuguese Foundation for Science and Technology (grant SFRH/BD/33465/2008).

Received: May 2, 2017

Revised: June 16, 2017

Accepted: June 30, 2017

Published: July 25, 2017

REFERENCES

- Ajami, B., Bennett, J.L., Krieger, C., Tetzlaff, W., and Rossi, F.M. (2007). Local self-renewal can sustain CNS microglia maintenance and function throughout adult life. *Nat. Neurosci.* *10*, 1538–1543.
- Askew, K., Li, K., Olmos-Alonso, A., Garcia-Moreno, F., Liang, Y., Richardson, P., Tipton, T., Chapman, M.A., Riecken, K., Beccari, S., et al. (2017). Coupled proliferation and apoptosis maintain the rapid turnover of microglia in the adult brain. *Cell Rep.* *18*, 391–405.
- Bergmann, O., Liebl, J., Bernard, S., Alkass, K., Yeung, M.S., Steier, P., Kutschera, W., Johnson, L., Landén, M., Druid, H., et al. (2012). The age of olfactory bulb neurons in humans. *Neuron* *74*, 634–639.
- Bernard, S., Frisén, J., and Spalding, K.L. (2010). A mathematical model for the interpretation of nuclear bomb test derived ¹⁴C incorporation in biological systems. *Nucl. Instrum. Methods Phys. Res. B* *268*, 1295–1298.
- Beura, L.K., Hamilton, S.E., Bi, K., Schenkel, J.M., Odumade, O.A., Casey, K.A., Thompson, E.A., Fraser, K.A., Rosato, P.C., Filali-Mouhim, A., et al. (2016). Normalizing the environment recapitulates adult human immune traits in laboratory mice. *Nature* *532*, 512–516.
- Bruttger, J., Karram, K., Wörtge, S., Regen, T., Marini, F., Hoppmann, N., Klein, M., Blank, T., Yona, S., Wolf, Y., et al. (2015). Genetic cell ablation reveals

- clusters of local self-renewing microglia in the mammalian central nervous system. *Immunity* 43, 92–106.
- Busch, R., Neese, R.A., Awada, M., Hayes, G.M., and Hellerstein, M.K. (2007). Measurement of cell proliferation by heavy water labeling. *Nat. Protoc.* 2, 3045–3057.
- Casano, A.M., and Peri, F. (2015). Microglia: multitasking specialists of the brain. *Dev. Cell* 32, 469–477.
- Eriksson, P.S., Perfilieva, E., Björk-Eriksson, T., Alborn, A.M., Nordborg, C., Peterson, D.A., and Gage, F.H. (1998). Neurogenesis in the adult human hippocampus. *Nat. Med.* 4, 1313–1317.
- Ernst, A., Alkass, K., Bernard, S., Salehpour, M., Perl, S., Tisdale, J., Possnert, G., Druid, H., and Frisé, J. (2014). Neurogenesis in the striatum of the adult human brain. *Cell* 156, 1072–1083.
- Ginhoux, F., Greter, M., Leboeuf, M., Nandi, S., See, P., Gokhan, S., Mehler, M.F., Conway, S.J., Ng, L.G., Stanley, E.R., et al. (2010). Fate mapping analysis reveals that adult microglia derive from primitive macrophages. *Science* 330, 841–845.
- Hoeffel, G., Chen, J., Lavin, Y., Low, D., Almeida, F.F., See, P., Beaudin, A.E., Lum, J., Low, I., Forsberg, E.C., et al. (2015). C-Myb(+) erythro-myeloid progenitor-derived fetal monocytes give rise to adult tissue-resident macrophages. *Immunity* 42, 665–678.
- Huttner, H.B., Bergmann, O., Salehpour, M., Rácz, A., Tatarishvili, J., Lindgren, E., Csonka, T., Csiba, L., Hortobágyi, T., Méhes, G., et al. (2014). The age and genomic integrity of neurons after cortical stroke in humans. *Nat. Neurosci.* 17, 801–803.
- Landsverk, O.J., Snir, O., Casado, R.B., Richter, L., Mold, J.E., Réu, P., Horneland, R., Paulsen, V., Yaqub, S., Aandahl, E.M., et al. (2017). Antibody-secreting plasma cells persist for decades in human intestine. *J. Exp. Med.* 214, 309–317.
- Lawson, L.J., Perry, V.H., and Gordon, S. (1992). Turnover of resident microglia in the normal adult mouse brain. *Neuroscience* 48, 405–415.
- Levin, I., Naegler, T., Kromer, B., Diehl, M., Francey, R.J., Gomez-Pelaez, A.J., Steele, L.P., Wagenbach, D., Weller, R., and Worthy, D.E. (2010). Observations and modelling of the global distribution and long-term trend of atmospheric $^{14}\text{CO}_2$. *Tellus B Chem. Phys. Meteorol.* 62, 26–46.
- Macallan, D.C., Wallace, D.L., Zhang, Y., Ghattas, H., Asquith, B., de Lara, C., Worth, A., Panayiotakopoulos, G., Griffin, G.E., Tough, D.F., and Beverley, P.C. (2005). B-cell kinetics in humans: rapid turnover of peripheral blood memory cells. *Blood* 105, 3633–3640.
- Mildner, A., Schmidt, H., Nitsche, M., Merkler, D., Hanisch, U.K., Mack, M., Heikenwalder, M., Brück, W., Priller, J., and Prinz, M. (2007). Microglia in the adult brain arise from Ly-6ChiCCR2+ monocytes only under defined host conditions. *Nat. Neurosci.* 10, 1544–1553.
- Miller, S.A., Dykes, D.D., and Polesky, H.F. (1988). A simple salting out procedure for extracting DNA from human nucleated cells. *Nucleic Acids Res.* 16, 1215.
- Neese, R.A., Misell, L.M., Turner, S., Chu, A., Kim, J., Cesar, D., Hoh, R., Antelo, F., Strawford, A., McCune, J.M., et al. (2002). Measurement in vivo of proliferation rates of slow turnover cells by $^2\text{H}_2\text{O}$ labeling of the deoxyribose moiety of DNA. *Proc. Natl. Acad. Sci. USA* 99, 15345–15350.
- Olah, M., Raj, D., Brouwer, N., De Haas, A.H., Eggen, B.J.L., Den Dunnen, W.F.A., Biber, K.P.H., and Boddeke, H.W.G.M. (2012). An optimized protocol for the acute isolation of human microglia from autopsy brain samples. *Glia* 60, 96–111.
- Parkhurst, C.N., Yang, G., Ninan, I., Savas, J.N., Yates, J.R., 3rd, Lafaille, J.J., Hempstead, B.L., Littman, D.R., and Gan, W.B. (2013). Microglia promote learning-dependent synapse formation through brain-derived neurotrophic factor. *Cell* 155, 1596–1609.
- Reimer, P.J., Brown, T.A., and Reimer, R.W. (2004). Discussion: reporting and calibration of post-bomb ^{14}C data. *Radiocarbon* 46, 1299–1304.
- Salehpour, M., Håkansson, K., and Possnert, G. (2013a). Accelerator mass spectrometry of ultra-small samples with applications in the biosciences. *Nucl. Instrum. Methods Phys. Res. B* 294, 97–103.
- Salehpour, M., Håkansson, K., Westermark, P., Antoni, G., Wikström, G., and Possnert, G. (2013b). Life science applications utilizing radiocarbon tracing. *Radiocarbon* 55, 865–873.
- Salehpour, M., Håkansson, K., and Possnert, G. (2015). Small sample accelerator mass spectrometry for biomedical applications. *Nucl. Instrum. Methods Phys. Res. B* 361, 43–47.
- Schulz, C., Gomez Perdiguero, E., Chorro, L., Szabo-Rogers, H., Cagnard, N., Kierdorf, K., Prinz, M., Wu, B., Jacobsen, S.E., Pollard, J.W., et al. (2012). A lineage of myeloid cells independent of Myb and hematopoietic stem cells. *Science* 336, 86–90.
- Shankaran, M., Marino, M.E., Busch, R., Keim, C., King, C., Lee, J., Killian, S., Awada, M., and Hellerstein, M.K. (2007). Measurement of brain microglial proliferation rates in vivo in response to neuroinflammatory stimuli: application to drug discovery. *J. Neurosci. Res.* 85, 2374–2384.
- Spalding, K.L., Bhardwaj, R.D., Buchholz, B.A., Druid, H., and Frisé, J. (2005). Retrospective birth dating of cells in humans. *Cell* 122, 133–143.
- Spalding, K.L., Bergmann, O., Alkass, K., Bernard, S., Salehpour, M., Huttner, H.B., Boström, E., Westerlund, I., Vial, C., Buchholz, B.A., et al. (2013). Dynamics of hippocampal neurogenesis in adult humans. *Cell* 153, 1219–1227.
- Stuiver, M., and Polach, H.A. (1977). Discussion reporting of ^{14}C data. *Radiocarbon* 19, 355–363.
- Tambuyzer, B.R., Ponsaerts, P., and Nouwen, E.J. (2009). Microglia: gatekeepers of central nervous system immunology. *J. Leukoc. Biol.* 85, 352–370.
- Tay, T.L., Mai, D., Dautzenberg, J., Fernández-Klett, F., Lin, G., Sagar, Datta, M., Drougard, A., Stempf, T., Ardura-Fabregat, A., et al. (2017). A new fate mapping system reveals context-dependent random or clonal expansion of microglia. *Nat. Neurosci.* 20, 793–803.
- Tonchev, A.B., Yamashima, T., Zhao, L., and Okano, H. (2003). Differential proliferative response in the posts ischemic hippocampus, temporal cortex, and olfactory bulb of young adult macaque monkeys. *Glia* 42, 209–224.
- Yeung, M.S., Zdunek, S., Bergmann, O., Bernard, S., Salehpour, M., Alkass, K., Perl, S., Tisdale, J., Possnert, G., Brundin, L., et al. (2014). Dynamics of oligodendrocyte generation and myelination in the human brain. *Cell* 159, 766–774.

Cell Reports, Volume 20

Supplemental Information

**The Lifespan and Turnover
of Microglia in the Human Brain**

Pedro Réu, Azadeh Khosravi, Samuel Bernard, Jeff E. Mold, Mehran Salehpour, Kanar Alkass, Shira Perl, John Tisdale, Göran Possnert, Henrik Druid, and Jonas Frisén

Supplemental Information - Mathematical modeling

“Bombcurve” age

A straightforward way to estimate the age of a sample is to subtract from the date of collection the calendar year of formation corresponding to the ^{14}C level of the sample. The corresponding “bombcurve” ages are a good estimate of the average age of the sample, when samples are not too old.

The birth-and-death equation

A more precise estimate of the age of a ^{14}C sample is obtained by using birth-and-death models. Birth-and-death models describe the dynamics (the evolution in time) of a cell population in an individual, in which cells are born and die. In an individual aged t years, we denote by $N(t)$ the *cell number* in the cell population. The atmospheric ^{14}C data provide information on the birthdates of the cells; it is natural to track the age of the cells. The *chronological age* of a cell is defined here as the time elapsed since its last division. To take into account the age of the cells, we break down the population $N(t)$ into a continuum of age bins. This introduces a population structured in chronological cell age a . The new dynamical variable $n(t,a)$ is the *cell density* at age a at time t . The *cell number* and the *cell density* are related in the following way

$$N(t) = \int_0^{\infty} n(t,a) da.$$

The cell density is expressed in *cells per year*. To specify fully the birth-and-death dynamics, we must set the *initial conditions*, the *birth rate* and the *death rate*. Each set of initial conditions, birth rate and death rate defines a model for the evolution of a cell population over the lifetime of an individual.

Homogeneous turnover model

The simplest model is the one where the cell number is fixed, and the birth and death rates are constant (**homogeneous turnover model**). All dying cells are replaced with a newborn cell, and all cells, old and young, are equally likely to be replaced. The cell death rate is the rate at which cells are replaced, and is termed turnover rate.

This model is well suited when the average age of the cells is relatively small (less than ~ 10 years). The “bombcurve” age estimate confirmed that the microglial cells were relatively young, with an average of 4.2 years. Because young samples are associated to high cell turnover, more complex models that take into account lifelong changes in turnover dynamics cannot be used. The birth-and-death equations for the homogeneous turnover model are

$$\underbrace{\frac{\partial n(t,a)}{\partial t}}_{\text{change in person age}} + \underbrace{\frac{\partial n(t,a)}{\partial a}}_{\text{change in cell age}} = \underbrace{-\gamma n(t,a)}_{\text{loss of cells}},$$

$$\text{(Initial condition)} \quad \underbrace{n(t=0,a)}_{\text{cells present at birth}} = \underbrace{N_0 \delta(a)}_{\text{all cells aged 0 at birth}},$$

$$\text{(Boundary condition)} \quad \underbrace{n(t,a=0)}_{\text{newborn cells}} = \underbrace{\gamma N_0}_{\text{cell birth}} \quad \text{for } t \in [0,t].$$

The first equation is a linear partial differential equation (PDE) that is often used in population dynamics (Perthame, 2007). It is a biological transport equation, with the term transport used in the sense that cells are transported along their age at a unit speed (i.e. they get older). The negative sign on the right-hand-side of the PDE indicates cell loss due to death. The initial condition states that cells are initially aged 0. The Dirac delta-function δ takes a value zero when a is not 0, and is normalized so that the total cell number

$$\int_0^{\infty} N_0 \delta(a) da = N_0.$$

According to the PDE, cells can only die but no source term for new cell is provided. We need to supplement the PDE with a special condition for newborn cells. The boundary condition specifies the birth rate of the cells ($n(t, a = 0)$). The equations are valid on domain $a \in [0,t]$, and $t \in [0,t]$, where t is the age of the individual at time of sample collection.

Heterogeneous turnover model

An alternative to the homogeneous model is a model where only a subset of the cells is susceptible to renewal. In that model, the homogeneous model is applied to a fraction f of the cell population, while a fraction $(1-f)$ is assigned a ^{14}C level corresponding to the year of birth of the donor.

Fitting the birth-and-death equations to the data

Computing the ^{14}C concentration associated to a model

Solutions for the cell density $n(t,a)$ can be expressed explicitly by (Bernard et al., 2010)

$$n(t,a) = N_0 \delta(t-a) e^{-\gamma a} + N_0 \gamma e^{-\gamma a}.$$

The first term accounts for the cells that were formed during development, and the second term accounts for the cells that were born after development. The total cell number, obtained by integrating $n(t,a)$ with respect to age a , is N_0 . The average ^{14}C level \tilde{C} of a DNA sample of a person born at calendar year D_{birth} and collected at calendar year D_{coll} , is

$$\tilde{C} = \frac{\int_0^{t=D_{\text{coll}}-D_{\text{birth}}} \overbrace{K_{\text{lag}}(D_{\text{coll}}-a)n(t,a)}^{\text{contribution of cells aged } a \text{ to } ^{14}\text{C}} da}{\underbrace{N(t)}_{\text{total number of cells}}}.$$

The function K_{lag} is a food-lag atmospheric ^{14}C level curve. When evaluated at calendar year y , $K_{\text{lag}}(y)$ represents the actual ^{14}C concentration that will integrate into new DNA, and will therefore correspond to an average of past atmospheric concentration, to account for the food supply chain, from photosynthesis to the table.

Here, we used a discrete shift function: $K_{\text{lag}}(y) = K(y - t_{\text{lag}})$ with $t_{\text{lag}} = 1$ year (Spalding et al., 2013). This means that the atmospheric carbon would take at time t_{lag} to reach dividing cells. ^{14}C content measured from blood serum in Swedish residents revealed a lag of 1.5 ± 0.7 years (Georgiadou et al., 2013), very close to the lag we used.

Individual turnover rates estimates with the homogeneous turnover model

The homogeneous model has a single parameter, the turnover rate γ , which can be estimated for each individual sample by solving the scalar equation $\tilde{C}(\gamma) = C_{\text{measured}}$ for γ . The initial cell number N_0 does not enter explicitly in the equation for \tilde{C} , since it appears as a factor on the numerator and the denominator.

Global estimates with the heterogeneous turnover model

The heterogeneous turnover model has two parameters, and cannot be fitted to individual donor, because there would not be a unique solution. Rather, the model was fitted to all the samples, and parameters estimated in the least-square sense, where the sum-of-square of the residuals $\sum (\tilde{C} - C_{\text{measured}})^2$ is minimized.

Numerical Methods

All simulations were performed with MATLAB (version R2012b). Solutions for the PDEs and the carbon concentration model were integrated numerically. The atmospheric ^{14}C level curve was sampled at mid-point each year (1993.5, 1994.5, ...) and linearly interpolated to convert it to a continuous function for use in the numerical integral functions.

Supplemental References

Bernard, S., Frisén, J., and spalding, K.L. (2010). A mathematical model for the interpretation of nuclear bomb test derived ^{14}C incorporation in biological systems. *Nucl Instr and Meth* 268, 1295-1298.

Georgiadou, E., Stenstrom, K.E., Uvo, C.B., Nilsson, P., Skog, G., and Mattsson, S. (2013). Bomb-pulse ^{14}C analysis combined with ^{13}C and ^{15}N measurements in blood serum from residents of Malmo, Sweden. *Radiation and environmental biophysics* 52, 175-187.

Perthame, B. (2007). Transport equations in biology. *Frontiers in Mathematics*.

Spalding, K.L., Bergmann, O., Alkass, K., Bernard, S., Salehpour, M., Huttner, H.B., Bostrom, E., Westerlund, I., Vial, C., Buchholz, B.A., *et al.* (2013). Dynamics of hippocampal neurogenesis in adult humans. *Cell* 153, 1219-1227.

Table S1 – Included subjects and IdU data, related to figure 1.

Donor	Age (years)	Cortical region	Per slide				Diagnosis	IdU administration (days)
			Iba1+ cells	Iba1+/IdU+ cells	% of IdU+ microglia	% of labeled cells / day		
Donor 1	17	frontal	1194	21	1,76	0,44	Metastatic Osteosarcoma. The dura and other meninges are unremarkable. The cerebrum contains 4 metastatic tumor nodules, all of which are superficial and form hard balls easily detached from the underlying cerebral tissue, which is compressed in those areas. From these nodules, one is located in the left frontal lobe measuring 1 x 1 cm, one in the left parietal lobe measuring 1. 5 x 1 cm and two in the occipital lobes bilaterally, measuring: 1 x 2 cm and 1. 5 x 3 cm correspondingly. The deeper cerebral substance and the cerebellum are free of tumor. Microscopy: The tumor nodule in the left parietal lobe appears pleomorphic. All nodules show an enormous amount of osteoid production. The osteoid is focally necrotic probably on a result to the radiotherapy.	4
			3224	15	0,47	0,12		
		occipital	2516	9	0,36	0,09		
			1479	9	0,61	0,15		
Donor 2	41	frontal	2573	3	0,12	0,01	Recurrent atrial fibro sarcoma (high-grade III sarcoma). Rare microscopic areas of recent ischemic infection in the cerebral cortex.	10
			1223	7	0,57	0,06		
		occipital	614	2	0,33	0,03		
			451	11	2,44	0,24		

0,8 0,14
AVERAGE AVERAGE

Table S2 – Included subjects and 14C data, related to figure 3.

Sample ID	Donor age (years)	Donor birth	Year of sample collection	Sex	Infections	Cause of death	Postmortem interval	Immuno labeling	Tissue	Estimated carbon mass according to measured DNA	Carbon mass measured in graphitization reactor
ND306	31	1983/05	2014	M	negative	NA	50,6h	CD45 ⁺ /CD11b ⁺	Cortex	8,87	8,54
ND308	69	1945/10	2014	M	negative	Accident (drown)	37h	CD45 ⁺ /CD11b ⁺	Cortex	36,80	29,64
ND311	52	1962/11	2014	M	negative	Suicide	25h	CD45 ⁺ /CD11b ⁺	Cortex	5,30	5,20
ND312	49	1965/04	2014	F	negative	Suicide (hanging)	51,9h	CD45 ⁺ /CD11b ⁺	Cortex	34,78	28,92
ND328	31	1983/06	2014	M	negative	Suicide (hanging)	49,4h	CD45 ⁺ /CD11b ⁺	Cortex	16,52	13,85
ND345	30	1985/03	2015	M	negative	Suicide (Intoxication)	37h	CD45 ⁺ /CD11b ⁺	Cortex	15,10	11,01
ND351	22	1993/04	2015	F	negative	Accident (Intoxication)	31h	CD45 ⁺ /CD11b ⁺	Cortex	2,98	2,77
ND353	58	1957/04	2015	F	negative	Accident	51h	CD45 ⁺ /CD11b ⁺	Cortex	5,98	5,50
ND357	65	1950/08	2015	M	negative	Coronary arteriosclerosis	45h	CD45 ⁺ /CD11b ⁺	Cortex	5,72	5,44
ND368	45	1971/11	2016	M	negative	Accident (Intoxication)	61h	CD45 ⁺ /CD11b ⁺	Cortex	7,73	6,50
ND373	44	1972/10	2016	M	negative	Suicide (hanging)	48h	CD45 ⁺ /CD11b ⁺	Cortex	4,03	2,81
ND374	33	1983/12	2016	M	negative	Suicide (hanging)	35h	CD45 ⁺ /CD11b ⁺	Cortex	8,40	6,29

Sample ID	Δ 14C (‰)	Δ 14C Error (2SD)	F 14C	F 14C Error (2SD)	NanoDrop A260	NanoDrop A280	NanoDrop 260/280	NanoDrop 260/230	Turnover rate (yearly)	Cell age (years)
ND306	52,28	18,40	1,060	0,018	1,06	0,54	1,96	2,20	0,199	5,0
ND308	48,62	16,20	1,057	0,016	4,42	2,25	1,96	2,26	0,236	4,2
ND311	71,88	38,20	1,080	0,038	0,64	0,34	1,89	2,11	0,122	8,2
ND312	56,91	18,40	1,065	0,018	4,18	2,10	1,99	2,26	0,172	5,8
ND328	43,45	20,20	1,052	0,020	1,98	1,01	1,96	2,22	0,322	3,1
ND345	30,20	18,60	1,038	0,019	1,81	0,90	2,02	2,28	1,056	0,9
ND351	10,41	45,80	1,018	0,046	0,36	0,18	1,94	2,13	Inf	0,0
ND353	-8,43	31,60	0,999	0,032	0,72	0,37	1,92	2,19	Inf	0,0
ND357	-24,93	34,40	0,983	0,034	0,69	0,35	1,97	2,38	Inf	0,0
ND368	25,22	31,67	1,033	0,032	0,93	0,49	1,91	2,29	1,084	0,9
ND373	107,53	35,25	1,116	0,035	0,48	0,26	1,90	2,23	0,070	13,6
ND374	59,81	26,46	1,068	0,026	1,01	0,52	1,93	2,32	0,122	8,1